Acta Crystallographica Section C
Crystal Structure Communications
ISSN 0108-2701

Hydrogen-bonding motifs and thermotropic polymorphism in redetermined halide salts of hexamethylenediamine

Charmaine van Blerk* and Gert J. Kruger

Department of Chemistry, University of Johannesburg, PO Box 524, Auckland Park, Johannesburg 2006, South Africa
Correspondence e-mail: cvanblerk@uj.ac.za

Received 18 June 2008
Accepted 21 July 2008
Online 20 September 2008

The redetermined crystal structures of hexane-1,6-diammonium dichloride, $C_6H_{18}N_2^{2+}\cdot 2Cl^-$, (I), hexane-1,6-diammonium dibromide, $C_6H_{18}N_2^{2+}\cdot 2Br^-$, (II), and hexane-1,6-diammonium diiodide, $C_6H_{18}N_2^{2+}\cdot 2I^-$, (III), are described, focusing on their hydrogen-bonding motifs. The chloride and bromide salts are isomorphous, with both demonstrating a small deviation from planarity [173.89 (10) and 173.0 (2)°, respectively] in the central C—C—C—C torsion angle of the hydrocarbon backbone. The chloride and bromide salts also show marked similarities in their hydrogen-bonding interactions, with subtle differences evident in the hydrogen-bond lengths reported. Bifurcated interactions are exhibited between the N-donor atoms and the halide acceptors in the chloride and bromide salts. The iodide salt is very different in molecular structure, packing and intermolecular interactions. The hydrocarbon chain of the iodide straddles an inversion centre and the ammonium groups on the diammonium cation of the iodide salt are offset from the planar hydrocarbon backbone by a torsion angle of 69.6 (4)°. All three salts exhibit thermotropic polymorphism, as is evident from differential scanning calorimetry analysis and variable-temperature powder X-ray diffraction studies.

Comment

Applications and structure–property relationships of *n*-alkyl diammonium salts are of continued interest and form the basis of our investigations. Our research focuses specifically on these materials as they are precursor ligands in transition metal complexes that have applications in propellants, explosives and pyrotechnic compositions (Singh *et al.*, 2005, 2006), and they have structure-directing properties in the synthesis of a number of nanoparticles (Chen *et al.*, 2007; Takami *et al.*, 2007).

The halide salts of hexamethylenediamine form the focus of this work. The structures of both the chloride salt, (I), and the bromide salt, (II), were initially determined almost 60 years ago (Binnie & Robertson, 1949*a*,*b*), and the chloride salt was redetermined 30 years ago (Borkakoti *et al.*, 1978). Some hydrogen-bonding details were published in Borkakoti's paper and our work expands further on the motifs and networks visible in the chloride salt. No further work on the structure of the bromide has been published since 1949 and no discussion of the hydrogen-bonding patterns was presented by Binnie and Robertson. The structure of the iodide salt, (III), was initially determined 45 years ago (Han, 1963) and no further work has since been reported for this material. We present in this paper the redetermined structures of all three halide salts, (I)–(III), and compare their hydrogen-bonding networks, motifs and interactions.

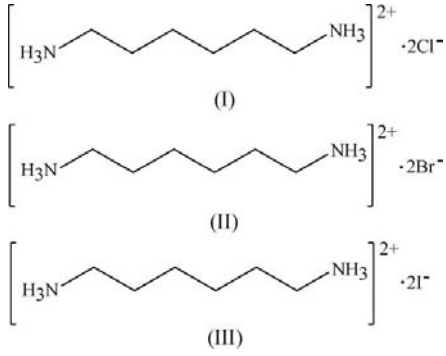

Fig. 1 depicts the molecular structures of all three compounds. The chloride and bromide salts are isomorphous, and a nonstandard unit cell (with a β angle less than 90°) was selected for the former so that the two salts would have compatible coordinates and so could be directly compared with each other. The asymmetric units of the chloride and bromide salts each consist of one hexane-1,6-diammonium cation and two halide anions. The diammonium cation chains deviate slightly from planarity, as can be seen from the torsion angles across C1—C2—C3—C4 (Tables 1 and 3). The iodide salt is markedly different from the other two halides in that its asymmetric unit consists of one-half of the hexane-1,6-diammonium cation and an iodide anion, with the hydrocarbon chain of the former straddling a crystallographic inversion centre. The ammonium groups of the iodide salt are offset from the planar hydrocarbon chain, as can be seen from the N1—C1—C2—C3 torsion angle (Table 5).

All three structures are hydrogen-bonded three-dimensional lattices. Figs. 2 and 3 depict the packing and the hydrogen-bonding motifs for both the chloride and bromide salts. Hydrogen-bond geometries for the chloride and bromide salts appear in Tables 2 and 4, respectively. There is evidence of bifurcated hydrogen-bonding interactions involving atoms H1*E* and H2*D* of the chloride salt (Table 2) and of the bromide salt (Table 4). Two of these contacts in both chloride and bromide salts (N1—H1*C*···Cl1^{ii}, N2—H2*D*···Cl1^{v}, N1—H1*C*···Br1^{ii} and N2—H2*D*···Br1^{v}) are almost out of the range of generally accepted hydrogen-bond distances and may be the consequences of stronger hydrogen-bonding interactions between the ammonium cation and the halide anion. The packing diagram and hydrogen-bonding motifs for the

 doi:10.1107/S0108270108022919

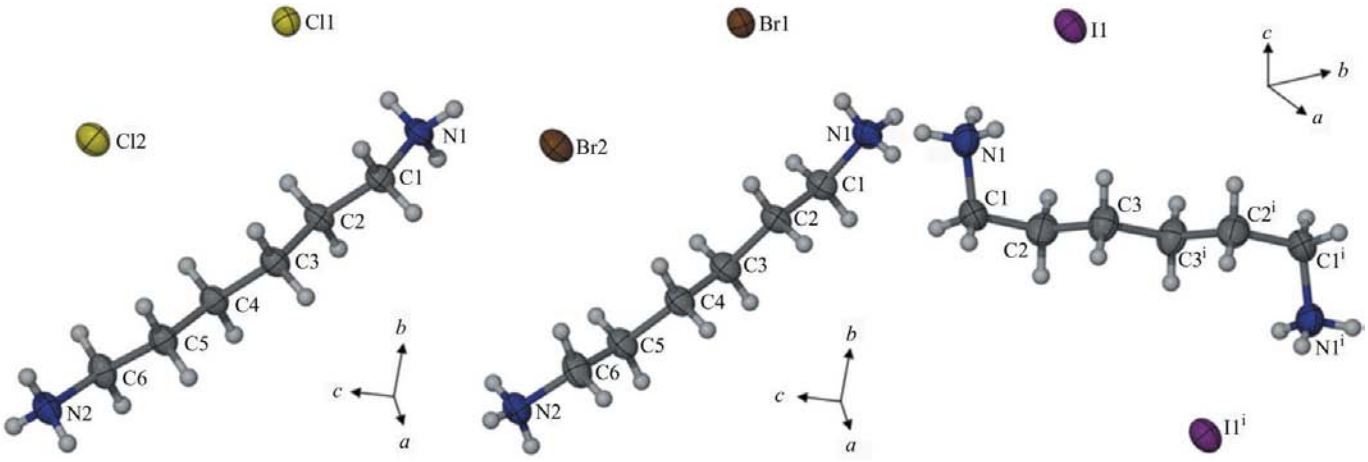

Figure 1
The molecular structures of (I) (left), (II) (centre) and (III) (right), showing the atomic numbering schemes. Displacement ellipsoids are drawn at the 50% probability level and H atoms are shown as small spheres of arbitrary radii. [Symmetry code: (i) $1-x, -y, 2-z$.]

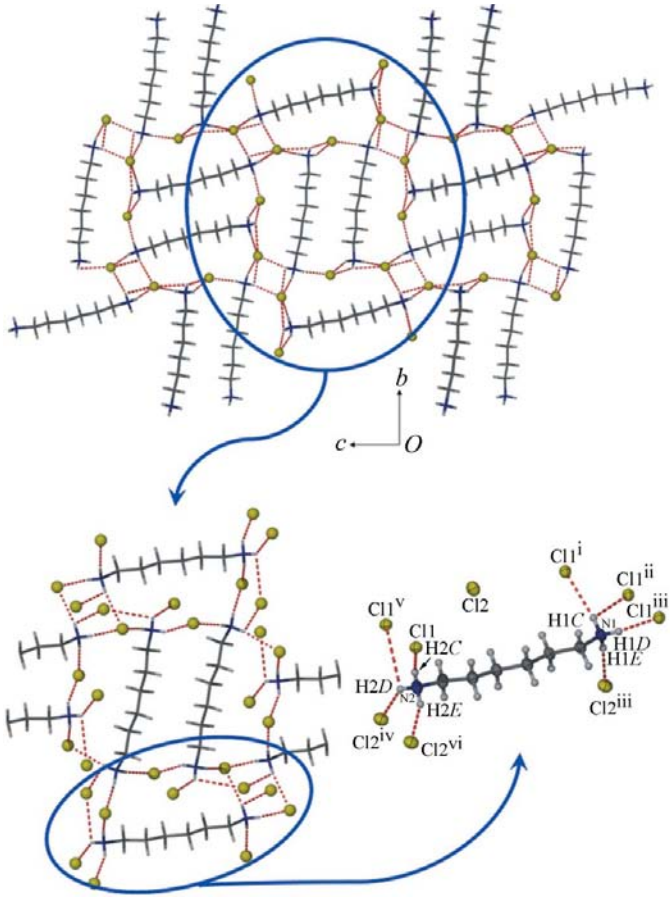

Figure 2
A packing diagram for (I), viewed down the *a* axis, showing the hydrogen-bonding network and motifs (top). A magnified view of the ring motifs (slightly offset from the *a* axis) is shown at the bottom left; selected cation chains have been truncated for clarity. A close-up view of the individual hydrogen-bonding contacts is shown at the bottom right. (Symmetry codes as in Table 2.)

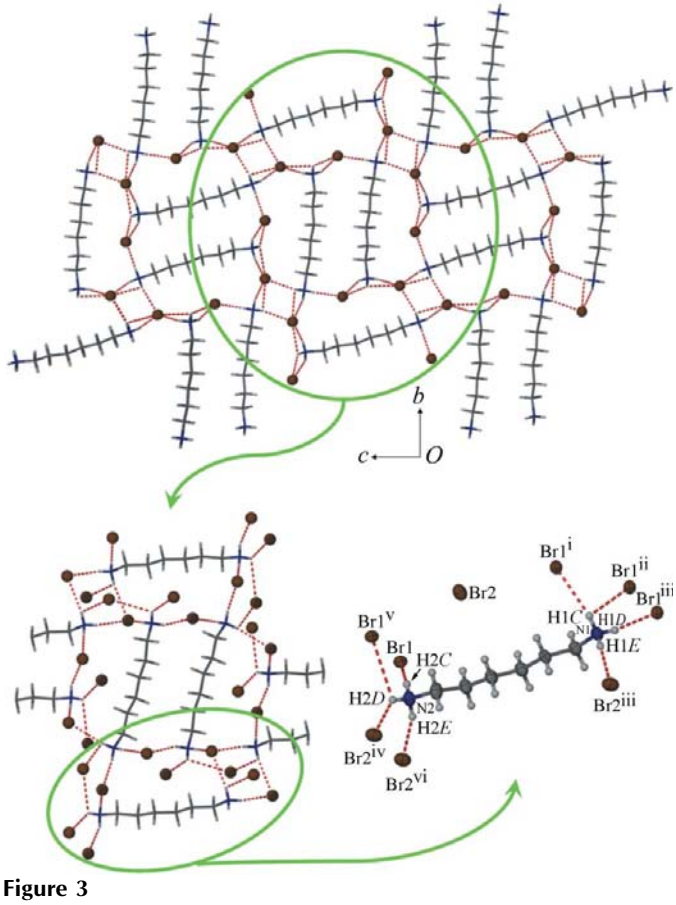

Figure 3
A packing diagram for (II), viewed down the *a* axis, showing the hydrogen-bonding network and motifs (top). A magnified view of the ring motifs (slightly offset from the *a* axis) is shown at the bottom left; selected cation chains have been truncated for clarity. A close-up view of the individual hydrogen-bonding contacts is shown at the bottom right. (Symmetry codes as in Table 2.)

iodide salt can be seen in Fig. 4, which is clearly different from the chloride and bromide salts. Details of the hydrogen-bond geometry for the iodide salt are given in Table 6.

Examination of the packing diagram of the chloride salt in Fig. 2 shows, at first glance, six different hydrogen-bonding ring motifs (top of Fig. 2, within the solid circle). All hydrogen-bonding motifs are described using graph-set notation

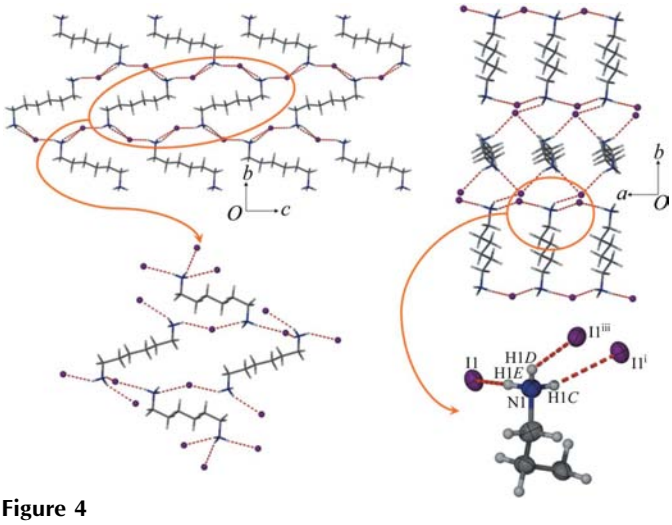

Figure 4
A packing diagram for (III), viewed down the *a* axis (top left) and down the *c* axis (top right), showing the hydrogen-bonding network and motifs. A magnified view of the 30-membered ring motif (slightly offset from the *a* axis) is shown at the bottom left. A close-up view of the asymmetric unit of (III) is given at the bottom right and shows the individual hydrogen-bonding contacts. (Symmetry codes as in Table 6.)

(Bernstein, 2002). There is one 19-membered ring (on the left within the solid circle) involving three diammonium cations and three chloride anions, with graph-set notation $R_4^3(19)$, one 22-membered ring (centre of the solid circle) involving two diammonium cations and two chloride anions, $R_4^2(22)$, and another 19-membered ring (on the right within the solid circle) involving three diammonium cations and three chloride anions, $R_4^3(19)$. The remaining three motifs appear to be an overlaid square, and diamond-shaped rings and multiple triangular rings, that when viewed slightly offset from the *a* axis and magnified (bottom left of Fig. 2) are actually interactions that link the packing sheets together. Further magnification of one diammonium cation clearly shows the eight individual hydrogen-bonding contacts (bottom right of Fig. 2) and demonstrates the bifurcation mentioned above.

An identical pattern exists for the bromide salt in Fig. 3 that shows, at first glance, six different hydrogen-bonding ring motifs (top of Fig. 3, within the solid circle). The same three

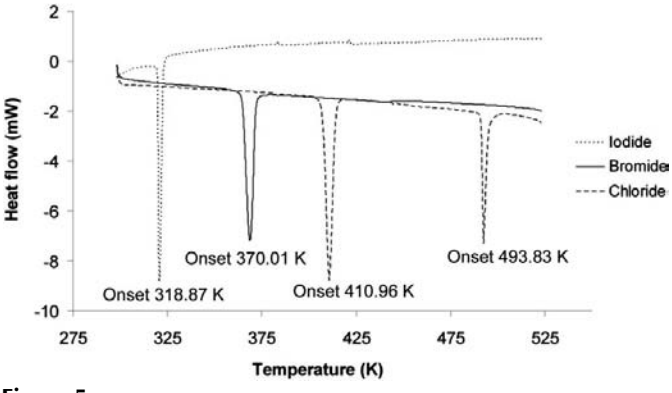

Figure 5
DSC traces of the three halide salts.

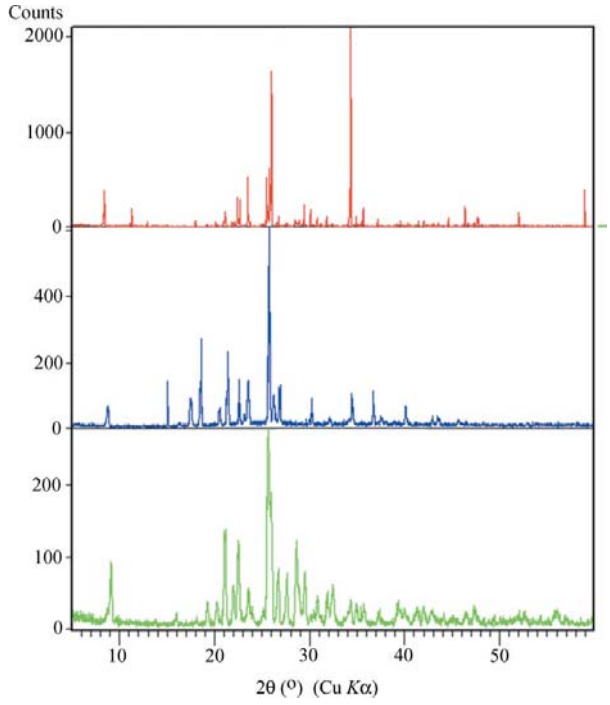

Figure 6
Comparative powder diffraction patterns of the chloride salt. The pattern at the top is of the material at the starting temperature of 303 K. The pattern in the middle is of the salt at 453 K after undergoing the phase change. The pattern at the bottom is of the salt after it has been cooled to the starting temperature.

ring motifs (two 19-membered rings and one 22-membered ring) that are described for the chloride salt also exist in the bromide salt. The remaining three motifs (overlaid square and diamond-shaped rings plus multiple triangular rings), when also viewed slightly offset from the *a* axis and magnified (bottom left of Fig. 3), are actually the interactions that link the packing sheets together. As with the chloride salt, further magnification of one diammonium cation clearly shows the eight individual hydrogen-bonding contacts (bottom right of Fig. 3).

Fig. 4 shows the packing diagram and hydrogen-bonding interactions for the iodide salt. A view of the packing down the *a* axis shows, at first glance, two different hydrogen-bonding ring motifs (top left of Fig. 4, within the solid circle). There is one large 30-membered ring involving four diammonium cations and four iodide anions, graph-set motif $R_6^4(30)$. The remaining motif is triangular and, when viewed slightly offset from the *a* axis and magnified (bottom left of Fig. 4), these are the interactions that link the packing layers together. A view of the packing down the *c* axis (top right of Fig. 4) reveals further 22-membered ring motifs that are shaped as elongated hexagons with the graph-set $R_4^2(22)$. The individual hydrogen-bonding contacts that link the layers are shown as a magnified view at the bottom right of Fig. 4, where the three hydrogen-bonding contacts in the asymmetric unit of the iodide salt are clearly evident.

The thermal properties of these salts were investigated by differential scanning calorimetry (DSC) and hot-stage micro-

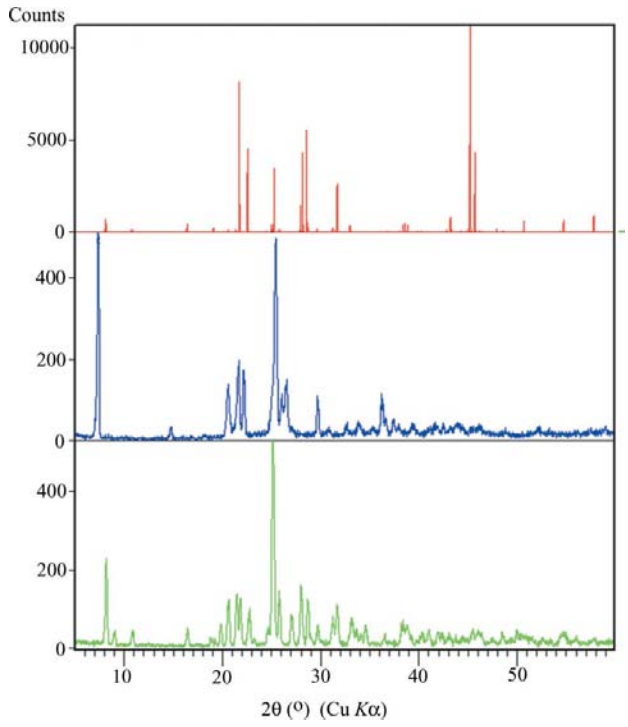

Figure 7
Comparative powder diffraction patterns of the bromide salt. The pattern at the top is of the material at the starting temperature of 303 K. The pattern in the middle is of the salt at 403 K after undergoing the phase change. The pattern at the bottom is of the salt after it has been cooled to the starting temperature.

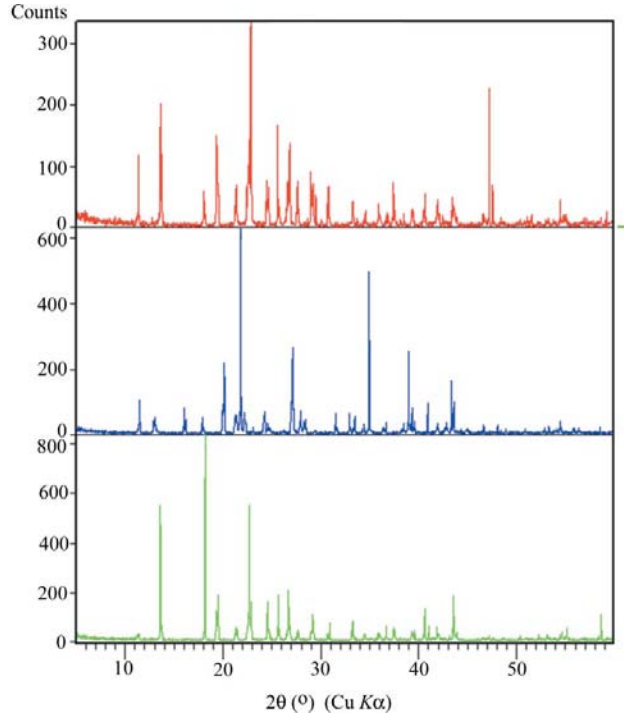

Figure 8
Comparative powder diffraction patterns of the iodide salt. The pattern at the top is of the material at the starting temperature of 303 K. The pattern in the middle is of the salt at 343 K after undergoing the phase change. The pattern at the bottom is of the salt after it has been cooled to the starting temperature.

scopy. Fig. 5 shows the DSC scans for all three halide salts. The chloride shows two endothermic events, while the bromide and iodide each show one. Hot-stage microscopy showed that the first endothermic event exhibits a change in morphology of the crystals, while the second, seen only in the chloride salt, is a sublimation at 493 K. Based on these observations, we decided to carry out variable-temperature powder diffraction (VT-PXRD) studies to establish if the changes in crystal morphologies are thermotropic phase changes. The VT-PXRD results for the chloride, bromide and iodide salts are shown in Figs. 6, 7 and 8, respectively. Each figure shows a powder pattern of the starting material at 303 K (top), a powder pattern of the material after the phase change at the respective high-temperature value (middle) and a powder pattern of the material on cooling to the starting temperature of 303 K (bottom). The results allow us to conclude that the endothermic events evident from the DSC data are in fact thermotropic phase changes. It is evident from the powder data that the chloride and bromide exhibit irreversible phase changes, which was also confirmed by the hot-stage microscopy. The iodide, however, exhibits a reversible phase change, as the two powder patterns at 303 K show the same peak positions. Further investigation is required in order to characterize the different phases.

Experimental

For the preparation of (I), concentrated hydrochloric acid (HCl, 2 ml, 63.6 mmol; Merck) was added to hexane-1,6-diamine (0.50 g, 4.30 mmol; Aldrich) in a sample vial. For the preparation of (II), concentrated hydrobromic acid (HBr, 2 ml, 37.07 mmol; Merck) was added to hexane-1,6-diamine (0.50 g, 4.30 mmol; Aldrich) in a sample vial. For the preparation of (III), concentrated hydriodic acid (HI, 2 ml, 26.58 mmol; Merck) was added to hexane-1,6-diamine (0.50 g, 4.30 mmol; Aldrich) in a sample vial. The three individual sample mixtures were refluxed at 363 K for 2 h. The three solutions were cooled to room temperature at a rate of 2 K h^{-1} and colourless crystals of hexane-1,6-diammonium dichloride, (I), hexane-1,6-diammonium dibromide, (II), and hexane-1,6-diammonium diiodide, (III), were formed. Suitable crystals of each salt were selected for study by single-crystal X-ray diffraction. The polycrystalline powders used for the variable-temperature powder diffraction studies were obtained by hand-milling each salt using an agate mortar and pestle.

The powder patterns for the three halide salts were collected on a PANalytical X'Pert PRO powder diffractometer (Cu $K\alpha$) fitted with an Anton Paar HTK1200 variable-temperature oven with an alumina sample cup. The powder patterns were collected at selected temperatures within the angular range $5 < 2\theta < 60^\circ$.

Compound (I)

Crystal data

$C_6H_{18}N_2^{2+}\cdot 2Cl^-$
M_r = 189.12
Monoclinic, $P2_1/c$
a = 4.6042 (1) Å
b = 14.1570 (3) Å
c = 15.6614 (4) Å
β = 89.327 (1)°
V = 1020.77 (4) Å^3
Z = 4
Mo $K\alpha$ radiation
μ = 0.58 mm^{-1}
T = 295 (2) K
0.48 × 0.20 × 0.18 mm

Data collection

Bruker SMART CCD diffractometer	10699 measured reflections
Absorption correction: multi-scan (*APEX2 AXScale*; Bruker, 2008)	2540 independent reflections
T_{min} = 0.769, T_{max} = 0.903	2195 reflections with $I > 2\sigma(I)$
	R_{int} = 0.021

Refinement

$R[F^2 > 2\sigma(F^2)]$ = 0.026	93 parameters
$wR(F^2)$ = 0.075	H-atom parameters constrained
S = 1.05	$\Delta\rho_{max}$ = 0.37 e Å^{-3}
2540 reflections	$\Delta\rho_{min}$ = −0.25 e Å^{-3}

Table 1
Selected torsion angles (°) for (I).

N1—C1—C2—C3	176.12 (10)	C3—C4—C5—C6	−176.27 (11)
C1—C2—C3—C4	−179.62 (10)	C4—C5—C6—N2	177.22 (10)
C2—C3—C4—C5	173.90 (10)		

Table 2
Hydrogen-bond and contact geometry (Å, °) for (I).

D—H···A	D—H	H···A	D···A	D—H···A
N1—H1C···Cl1^{i}	0.89	2.43	3.2599 (11)	156
N1—H1C···Cl1^{ii}	0.89	2.94	3.3754 (10)	112
N1—H1D···Cl1^{iii}	0.89	2.32	3.2000 (10)	168
N1—H1E···Cl2^{iii}	0.89	2.29	3.1695 (10)	172
N2—H2C···Cl1	0.89	2.33	3.1765 (10)	158
N2—H2D···Cl2^{iv}	0.89	2.43	3.1616 (10)	139
N2—H2D···Cl1^{v}	0.89	3.18	3.5361 (11)	107
N2—H2E···Cl2^{vi}	0.89	2.31	3.1511 (11)	157

Symmetry codes: (i) $-x+1, y+\frac{1}{2}, -z+\frac{3}{2}$; (ii) $x+1, -y+\frac{1}{2}, z-\frac{1}{2}$; (iii) $x, -y+\frac{1}{2}, z-\frac{1}{2}$; (iv) $-x+2, y-\frac{1}{2}, -z+\frac{3}{2}$; (v) $x+1, y, z$; (vi) $-x+1, y-\frac{1}{2}, -z+\frac{3}{2}$.

Compound (II)

Crystal data

$C_6H_{18}N_2^{2+}\cdot 2Br^-$	V = 1104.92 (4) Å^3
M_r = 278.04	Z = 4
Monoclinic, $P2_1/c$	Mo $K\alpha$ radiation
a = 4.7044 (1) Å	μ = 7.28 mm^{-1}
b = 14.4462 (3) Å	T = 295 (2) K
c = 16.2582 (4) Å	0.44 × 0.26 × 0.10 mm
β = 90.115 (1)°	

Data collection

Bruker SMART CCD diffractometer	19693 measured reflections
Absorption correction: multi-scan (*APEX2 AXScale*; Bruker, 2008)	2753 independent reflections
T_{min} = 0.117, T_{max} = 0.483	2364 reflections with $I > 2\sigma(I)$
	R_{int} = 0.042

Refinement

$R[F^2 > 2\sigma(F^2)]$ = 0.025	94 parameters
$wR(F^2)$ = 0.060	H-atom parameters constrained
S = 1.05	$\Delta\rho_{max}$ = 0.84 e Å^{-3}
2753 reflections	$\Delta\rho_{min}$ = −0.65 e Å^{-3}

Table 3
Selected torsion angles (°) for (II).

N1—C1—C2—C3	175.8 (2)	C3—C4—C5—C6	−175.4 (2)
C1—C2—C3—C4	−179.7 (2)	C4—C5—C6—N2	176.6 (2)
C2—C3—C4—C5	173.0 (2)		

Table 4
Hydrogen-bond and contact geometry (Å, °) for (II).

D—H···A	D—H	H···A	D···A	D—H···A
N1—H1C···Br1^{i}	0.89	2.56	3.408 (2)	159
N1—H1C···Br1^{ii}	0.89	3.11	3.529 (2)	111
N1—H1D···Br1^{iii}	0.89	2.47	3.3466 (19)	168
N1—H1E···Br2^{iii}	0.89	2.43	3.313 (2)	174
N2—H2C···Br1	0.89	2.50	3.330 (2)	156
N2—H2D···Br2^{iv}	0.89	2.59	3.299 (2)	137
N2—H2D···Br1^{v}	0.89	3.09	3.505 (2)	111
N2—H2E···Br2^{vi}	0.89	2.47	3.310 (2)	158

Symmetry codes: as in Table 2.

Compound (III)

Crystal data

$C_6H_{18}N_2^{2+}\cdot 2I^-$	V = 613.58 (3) Å^3
M_r = 372.02	Z = 2
Monoclinic, $P2_1/c$	Mo $K\alpha$ radiation
a = 4.8884 (1) Å	μ = 5.08 mm^{-1}
b = 12.8756 (4) Å	T = 295 (2) K
c = 9.7488 (3) Å	0.48 × 0.18 × 0.18 mm
β = 90.423 (2)°	

Data collection

Bruker SMART CCD diffractometer	5135 measured reflections
Absorption correction: integration (*XPREP*; Bruker, 2008)	1551 independent reflections
T_{min} = 0.194, T_{max} = 0.462	1452 reflections with $I > 2\sigma(I)$
	R_{int} = 0.028

Refinement

$R[F^2 > 2\sigma(F^2)]$ = 0.024	48 parameters
$wR(F^2)$ = 0.059	H-atom parameters constrained
S = 1.09	$\Delta\rho_{max}$ = 1.24 e Å^{-3}
1551 reflections	$\Delta\rho_{min}$ = −0.51 e Å^{-3}

Table 5
Selected torsion angles (°) for (III).

N1—C1—C2—C3	69.6 (4)	C1—C2—C3—C3^{i}	−178.3 (4)

Symmetry code: (i) $-x, -y, -z+2$.

Table 6
Hydrogen-bond geometry (Å, °) for (III).

D—H···A	D—H	H···A	D···A	D—H···A
N1—H1C···I1^{ii}	0.89	2.76	3.617 (3)	163
N1—H1D···I1^{iii}	0.89	2.79	3.586 (3)	149
N1—H1E···I1	0.89	2.91	3.666 (3)	144

Symmetry codes: (ii) $x-1, y, z$; (iii) $x-1, -y+\frac{1}{2}, z-\frac{1}{2}$.

H atoms were positioned geometrically and refined in the riding-model approximation, with C—H = 0.97 Å and N—H = 0.89 Å, and with U_{iso}(H) = 1.2U_{eq}(C) or 1.5U_{eq}(N). For (III), the highest peak of 1.24 e Å^{-3} in the final difference map lies 0.75 Å from atom I1.

For all compounds, data collection: *SMART-NT* (Bruker, 1999); cell refinement: *SAINT* (Bruker, 2008); data reduction: *SAINT* (Bruker, 2008); program(s) used to solve structure: *SHELXS97* (Sheldrick, 2008); program(s) used to refine structure: *SHELXL97* (Sheldrick, 2008); molecular graphics: *X-SEED* (Barbour, 2001) and

Mercury (Macrae *et al.*, 2006); software used to prepare material for publication: *PLATON* (Spek, 2003) and *publCIF* (Westrip, 2008).

The authors acknowledge the University of Johannesburg and the NRF Thuthuka Programme for funding for this study, and the University of the Witwatersrand for the use of the single-crystal diffractometer in the Jan Boeyens Structural Chemistry Laboratory.

Supplementary data for this paper are available from the IUCr electronic archives (Reference: BM3056). Services for accessing these data are described at the back of the journal.

References

Barbour, L. J. (2001). *J. Supramol. Chem.* **1**, 189–191.
Bernstein, J. (2002). *Polymorphism in Molecular Crystals*, pp. 55–57. New York: Oxford University Press.
Binnie, W. P. & Robertson, J. M. (1949*a*). *Acta Cryst.* **2**, 116–120.
Binnie, W. P. & Robertson, J. M. (1949*b*). *Acta Cryst.* **2**, 180–188.
Borkakoti, N., Lindley, P. F., Moss, D. S. & Palmer, R. A. (1978). *Acta Cryst.* B**34**, 3431–3433.
Bruker (1999). *SMART-NT*. Version 5.050. Bruker AXS Inc., Madison, Wisconsin, USA.
Bruker (2008). *APEX2 AXScale*, *SAINT* and *XPREP*. Versions 2008/2-0. Bruker AXS Inc., Madison, Wisconsin, USA.
Chen, F., Zhu, K., Gan, G. J., Shen, S. & Kooli, F. (2007). *Mater. Res. Bull.* **42**, 1128–1136.
Han, K. (1963). *J. Korean Chem. Soc.* **7**, 74–84.
Macrae, C. F., Edgington, P. R., McCabe, P., Pidcock, E., Shields, G. P., Taylor, R., Towler, M. & van de Streek, J. (2006). *J. Appl. Cryst.* **39**, 453–457.
Sheldrick, G. M. (2008). *Acta Cryst.* A**64**, 112–122.
Singh, G., Singh, C. P. & Mannan, S. M. (2005). *Thermochim. Acta*, **437**, 21–25.
Singh, G., Singh, C. P. & Mannan, S. M. (2006). *J. Hazard. Mater.* **135**, 10–14.
Spek, A. L. (2003). *J. Appl. Cryst.* **36**, 7–13.
Takami, S., Sato, T., Mousavand, T., Ohara, S., Umetsu, M. & Adschiri, T. (2007). *Mater. Lett.* **61**, 4769–4772.
Westrip, S. P. (2008). *publCIF*. In preparation.